Energy dissipation mechanisms in the FCPb light-harvesting complex of the diatom *Cyclotella meneghiniana*

Huzifa M.A.M. Elnour[1], Lars Dietzel[2], Charusheela Ramanan[3], Claudia Büchel[2], Rienk van Grondelle[3], Tjaart PJ Krüger[1*]

[1]Department of Physics, University of Pretoria, Pretoria, South Africa

[2]Institute of Molecular Biosciences, Goethe University Frankfurt, Frankfurt, Germany

[3]Department of Physics, VU University, Amsterdam, The Netherlands

[*]To whom correspondence should be addressed; E-mail: tjaart.kruger@up.ac.za

August 15, 2018

Abstract

Transient absorption spectroscopy has been applied to investigate the energy dissipation mechanisms in the nonameric fucoxanthin-chlorophyll-a,c-binding protein FCPb of the centric diatom *Cyclotella meneghiniana*. FCPb complexes in their unquenched state were compared with those in two types of quenching environments, namely aggregation-induced quenching by detergent removal, and clustering via incorporation into liposomes. Applying global and target analysis, in combination with a fluorescence lifetime study and annihilation calculations, we were able to resolve two quenching channels in FCPb that involve chlorophyll-a pigments for FCPb exposed to both quenching environments. The fast quenching channel operates on a timescale of tens of picoseconds and exhibits similar spectral signatures as the unquenched state. The slower quenching channel operates on a timescale of tens to hundreds of picoseconds, depending on the degree of quenching, and is characterized by enhanced population of low-energy states between 680 and 710 nm. The results indicate that FCPb is, in principle, able to function as a dissipater of excess energy and can do this *in vitro* even more efficiently than the homologous FCPa complex, the sole complex involved in fast photoprotection in these organisms. This indicates that when a complex displays photoprotection-related spectral signatures *in vitro* it does not imply that the complex participates in photoprotection *in vivo*. We suggest that FCPa is favored over FCPb as the sole energy-regulating complex in diatoms because its composition can more easily establish the balance between light-harvesting and quenching required for efficient photoprotection.

keywords

Diatom

Light harvesting antenna

proteoliposome

fucoxanthin-chlorophyll protein

Nonphotochemical quenching

Transient absorption spectroscopy

Highlights

- FCPb possesses two distinct quenching mechanisms involving chlorophyll-a
- The slow quenching mechanism displays strongly red-shifted absorption
- *In vitro*, FCPb is a more efficient energy dissipater than FCPa
- *In vivo*, FCPb does not regulate energy due to its lack of a pH sensor
- Proteoliposomes are better photoprotection model systems than aggregation

1. Introduction

Diatoms are unicellular photosynthetic organisms. They play an important role in the biochemical cycles of nitrogen, silicon, phosphorus and carbon, and, consequently, have a great impact on the global climate in marine and freshwater environments [1]. The light-harvesting complexes (LHCs) of diatoms belong to the same extended family as those of higher plants and green algae [2]. However, there are some clear differences in their protein and pigment compositions [3, 4]. Diatoms bind up to 8 chlorophyll-a (Chl-a) pigments per monomer [5], as in the main light-harvesting complexes of plants, LHCII [6]. However, diatoms bind Chl-c instead of the Chl-b found in LHCII. Furthermore, diatoms comprise unique types of carotenoids. The main carotenoid is fucoxanthin (Fx) and is present in a similar quantity as Chl-a [7], giving diatoms a brown colour and their LHCs the name of fucoxanthin-Chl-a,c-binding protein (FCP). FCPs additionally bind the xanthophyll-cycle pigments diadinoxanthin (Dd) and diatoxanthin (Dt) in substoichiometric amounts.

The two main types of FCP purified from centric diatoms like *Cyclotella meneghiniana* are known as FCPa and FCPb [4]. They mainly differ in their polypeptide composition and oligomeric state. FCPa is a trimer consisting of a mixture of the

polypeptides Fcp1-3 from the Lhcf family and an Lhcx polypeptide in a smaller quantity, whereas FCPb assumes a nonameric arrangement [8] of Fcp5, a different type of Lhcf polypeptide [3]. The amount of Lhcx per FCPa scales with the light intensity incident on the diatoms and this polypeptide plays an important role in photoprotection [9]. Specifically, the photoprotection process known as nonphotochemical quenching (NPQ) of Chl-a fluorescence is triggered by a low lumenal pH and it is also associated with a high Dt content [4, 10–12]. The fluorescence yield of isolated FCPa complexes was shown to depend strongly on the Dt content and the environmental pH, while FCPb was found to be insensitive to such changes [13, 14]. FCPa is therefore widely considered to be the site of qE, the dominant, fast, energy-dependent, reversible component of NPQ, while FCPb is regarded to be merely involved with light harvesting.

Since the early studies of NPQ in higher plants, aggregation of light-harvesting complexes has been a useful model for the investigation of qE [15–19]. More recently, this approach was also used to investigate qE in diatoms [13, 14, 20]. Evidence of aggregation in the membranes of higher plants has been found under NPQ conditions [21–23]. Moreover, the fluorescence from isolated FCPa complexes was strongly reduced upon decrease of the ambient pH, likely due to spontaneous aggregation, while a lower pH only marginally reduced the fluorescence from isolated FCPb complexes, possibly due to their aggregation state remaining unaltered [13]. Based on the above-mentioned evidence, NPQ models in diatoms have considered aggregation of FCPa complexes in the membrane as one of the excited-state quenching mechanisms [14, 24–26].

Time-resolved fluorescence measurements on whole high-light acclimated diatoms at room temperature have revealed two spectroscopic signatures of their NPQ state: a bathochromic shift of their fluorescence emission spectrum and enhanced emission between 700 and 750 nm, in the tail of the spectrum [24, 25]. These signatures were proposed to originate from the formation of FCPa aggregates [14]. In addition, 77 K steady-state fluorescence spectra of FCPa aggregates induced *in vitro* showed similar spectral features [25], but so do the spectra of FCPb aggregates [14]. In fact, the low-energy emission from FCPb aggregates is more pronounced than for FCPa aggregates [14] and may have an important contribution to the low-energy emission of diatoms under NPQ conditions. A Stark fluorescence spectroscopy study on FCPa and FCPb complexes revealed the appearance of a low-energy band peaking between 692 and 694 nm upon aggregation of both complexes [27]. The same study showed that FCPa aggregates exhibit an additional, more red-shifted emission band (peaking at 740 nm) and it was argued that FCPb complexes may display a similar behaviour *in vivo* [27].

Different thermal energy dissipative processes have been revealed through fluorescence and absorption studies [14, 24, 25, 27–29], suggesting that qE is very likely established in diatoms through the combination of multiple processes involving different sites. The kinetics and spectral properties of quenching processes in FCPa involving Chl-a pigments were investigated in a

recent room-temperature transient-absorption study of FCPa complexes in their solubilized and aggregated states, using selective Chl-a excitation [30]. Here, we apply a similar approach to FCPb in order to characterize the quenching processes in these complexes and to determine the similarities and differences compared to quenching processes taking place in FCPa. Quenching of FCPb was induced in two different ways, namely through strong aggregation by detergent removal, and by incorporating the complexes into liposomes of natural lipids with a high protein-to-lipid ratio. The latter represents a milder environment, giving rise to smaller clusters [31], and provides a better representation of the native environment of the complexes. Global and target analysis was applied to the data to resolve the energy transfer kinetics and timescales, with a particular focus on quenching states. In addition to singlet-singlet annihilation, we were able to resolve two quenching channels associated with different molecular mechanisms in FCPb and we identified their associated transient spectra and operation timescales.

2. Materials and methods

2.1. Sample preparation

Cyclotella meneghiniana (Culture Collection Göttingen, strain 1020-1a) was grown in artificial seawater [32] supplemented with 2 mM silica, in low light conditions (40 μmol photons $m^{-2}s^{-1}$, 16 h light, 8 h dark) with temperatures kept between 15-17 °C. Cells were harvested after one week of cultivation in the light-adapted state. FCPb isolation was carried out as described in [14]. In brief, thylakoids were isolated with a beadmill followed by an ultracentrifugation step. Thylakoids corresponding to 250 μg Chl-a ml^{-1} were solubilized with 20 mM β-dodecylmaltoside (β–DM) and subjected to ion exchange chromatography followed by ultracentrifugation using a freeze thaw gradient (19% sucrose (w/v), 25 mM Tris, pH 7.4, 2 mM KCl and 0.03 % (w/v) βDM). The collected FCPb fraction was washed in 25 mM Tris, 2 mM KCl, pH 7.4 and concentrated via ultrafiltration (centripreps, 30 kD cutoff). Liposomes were prepared as described in [31], using plant thylakoid lipids (Larodan Fine Chemicals, Sweden) with a Chl-a-to-lipid molar ratio of 12. Figure S1 shows the separation of purified FCPb complexes used in this study. FCPb aggregates were prepared by removing the detergent with bio-beads (SM-2 adsorbent, Bio-Rad) during continuous magnetic stirring and monitoring of the fluorescence intensity. The fluorescence yield of the aggregated FCPb was reduced by a factor of ten, after which the bio-beads were removed via centrifugation.

2.2. Spectroscopic methods

2.2.1 Steady-state spectroscopy

Steady-state absorption spectra were recorded with a Lambda 40 UV/VIS spectrometer (Perkin-Elmer) from 350 nm to 750 nm using 1 mm path length cuvettes. The fluorescence emission spectra were recorded with a Fluoromax-3 Horiba from 600 nm to 800 nm, upon excitation at 465 nm. For the fluorescence emission measurements, cuvettes with a 1 cm path length were

used and samples were diluted to an OD of 0.05 at the maximum of the Chl-a Q_y band.

2.2.2 Fluorescence lifetime measurements

Time-resolved fluorescence measurements were performed using a FluoTime 200 fluorometer (PicoQuant). The samples were diluted into the appropriate buffer to an OD of 0.05 at the Q_y maximum of 672 nm and stirred in a cuvette with a path length of 1 cm. Excitation was provided by a 468 nm diode laser with a repetition rate of 10 MHz and energy of 8 nJ/pulse. The instrument response function (IRF) was obtained with pinacyanol iodide dissolved in methanol, which has a fluorescence lifetime of 6 ps [33]. Emitted fluorescence was recorded at 675 nm at an angle of 90° with respect to the excitation. All measurements were performed at ambient temperature, and the maximum number of counts in the peak channel was 20,000. The full width at half maximum of the IRF was 88 ps.

2.2.3 Transient absorption spectroscopy

Femtosecond transient absorption (TA) spectroscopy on the FCPb complexes incorporated into liposomes (plFCPb) and FCPb aggregates (qFCPb) was conducted with a pump-probe setup described in ref. [34], while annihilation studies on the solubilized FCPb (sFCPb) were performed on a setup described in ref. [35]. The main difference between the two setups is the laser source. The first setup [34] uses 80 fs laser pulses at a wavelength of 800 nm, obtained from a Ti:sapphire oscillator-regenerative amplifier (Coherent Mira seed and RegA) operating at a 40 kHz repetition rate. The second setup [35] is driven by an ultrashort 50 fs laser pulse at the wavelength of 800 nm at 1 kHz repetition rate, generated also from a Ti:sapphire oscillator (Coherent Mira seed) and amplified with a kilohertz amplifying system (Alpha-1000 US, B.M.Industries). For both setups, the pump beam wavelength was tuned to 680 nm and its polarization was set at the magic angle (54.7°) with respect to the probe beam polarization. The TA spectra were collected at pump energies of 6 nJ/pulse and 10 nJ/pulse for the plFCPb sample, whereas 10 nJ/pulse was used for qFCPb. In order to perform singlet-singlet (S-S) annihilation studies on the sFCPb sample, we used pump energies of 10, 20 and 30 nJ/pulse. The time evolution of the number of excitations $n(t)$ is given by [36, 37]:

$$\frac{\mathrm{dn(t)}}{\mathrm{dt}} = -\frac{1}{\tau}\mathrm{n(t)} - \gamma \mathrm{n(t)}^2 \tag{1}$$

which has the analytical solution

$$\mathrm{n(t)} = \frac{\mathrm{n_0 e^{(-t/\tau)}}}{1 + \frac{1}{2}\mathrm{n_0}\gamma\tau(1 - \mathrm{e^{(-t/\tau)}})} \tag{2}$$

where n is the number of excited nonamers per pulse at a time t after excitation, with $\mathrm{n(t=0)} = \mathrm{n_0} = \mathrm{I}\sigma$ being the initial number of excitations per pulse, I the intensity of the pump beam and σ the absorption cross-section of an FCPb nonamer.

γ is the rate of S-S annihilation, and τ the lifetime of an exponential decay component. This kinetic method for the S-S annihilation study is valid for supermolecules such as small LHCII aggregates, which have a size greater than or equal to the excitation diffusion length [36, 37]. Due to the relatively large size of the FCPb complex, we assumed the same approach for this complex. The samples were inserted in a 1 mm path length cuvette, which was mounted on a shaker to prevent sample degradation from over-exposure due to multiple laser shots. Sample ODs were adjusted to 0.5 at the Chl-a Q_y absorption maximum. All measurements were conducted at room temperature (RT). Absorption spectra were taken before and after the TA measurements to monitor the stability of the samples. Global and Target Analysis [38, 39] was applied to analyze the TA spectroscopy data.

3. Results

3.1. Steady-state absorption and fluorescence emission spectra

The abbreviations sFCPb, plFCPb, and qFCPb will be used to denote solubilized FCPb nonamers, FCPb nonamers incorporated into liposomes and aggregated (quenched) FCPb complexes, respectively. The room-temperature steady-state absorption and fluorescence emission spectra of these complexes are displayed in Figure 1. The Soret and Q_y absorption bands of Chl-a are centered around 438 and 670 nm, respectively, whereas those for Chl-c are visible as a shoulder at 455 nm and a small band at 635 nm, respectively. The broad tail between 480 and 575 nm is principally due to the $S_0 \rightarrow S_2$ transition of fucoxanthin molecules and a minor contribution from the xanthophyll-cycle pigments, mainly diadinoxanthin. The spectral features correspond well with previous reports [3, 4, 20]. The liposome environment as well as aggregation induced significant broadening of the Soret band towards higher energies (i.e. shorter wavelength) and a slight enhancement in the tail of the Q_y band towards the red (Figure 1(a) inset). Similar broadening was observed for FCPa aggregates in a previous study [30]. The somewhat reduced amplitude between 500 and 560 nm and around 635 nm for qFCPb is likely due to pigment loss during bio-bead treatment to induce aggregation.

The fluorescence emission spectra of FCPb (Figure 1(b)) in all three investigated environments show a maximum at 674 nm and a vibrational band at around 735 nm. Since all pigments in the complex can be excited at 465 nm, the spectral shape is indicative of efficient excitation energy transfer to Chl-a [7]. The lack of significant differences between the spectra indicates that aggregation and incorporation into liposomes did not affect the steady-state spectroscopic properties of the pigments in FCPb, with the exception of the fluorescence lifetimes (*vide infra*). The slight broadening of the spectra of qFCPb and pIFCPb can be explained by scattering from aggregates.

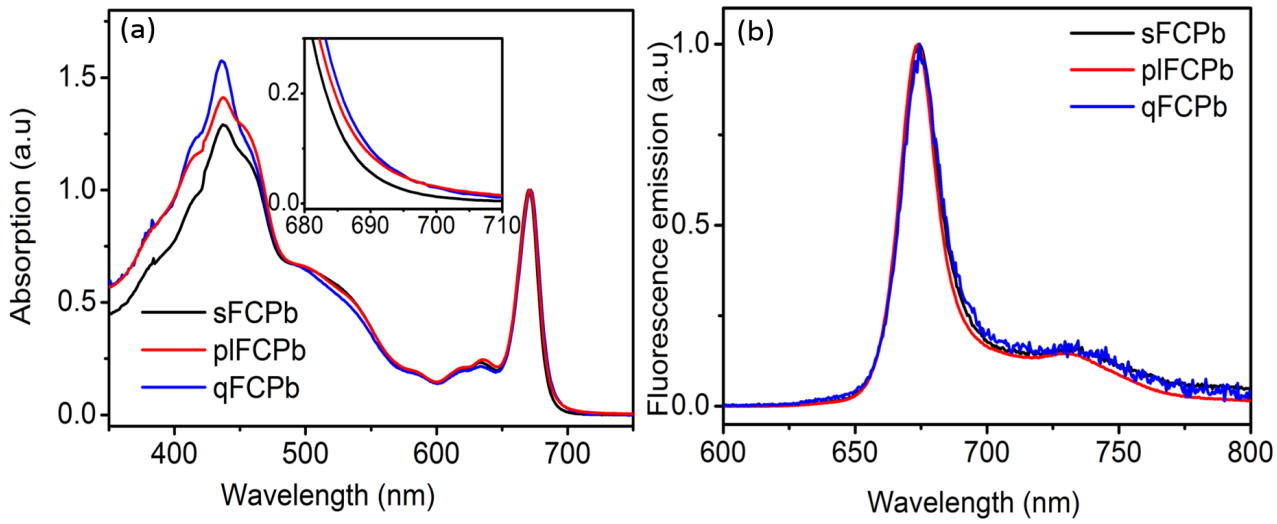

Figure 1: Steady-state (a) absorption and (b) fluorescence emission spectra upon excitation at 465 nm of sFCPb (black), plFCPb (red) and qFCPb (blue), normalized to the Chl-a Q_y band. Inset in (a) displays the same spectrum between 680 and 710 nm.

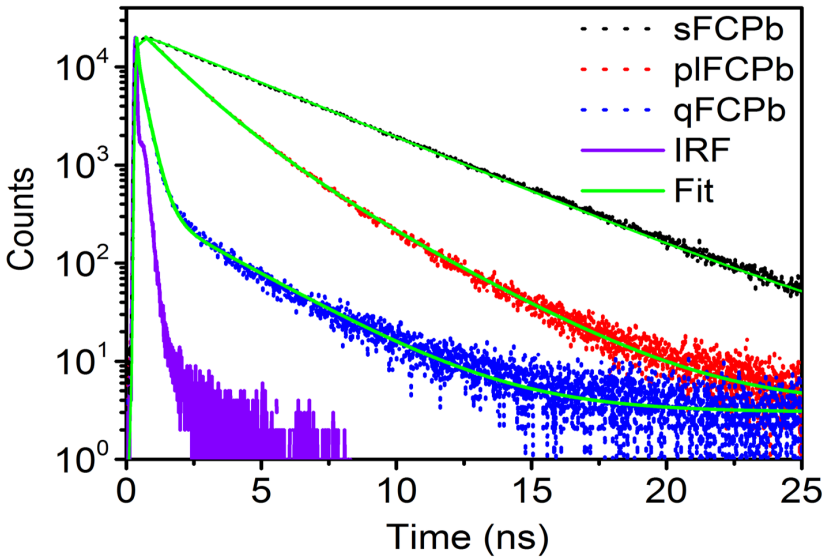

Figure 2: Fluorescence decay curves of sFCPb (black), plFCPb (red), qFCP (blue), Fit (green) and IRF (violet) detected at 675 nm at room temperature upon excitation at 468 nm. IRF denotes instrument response function.

3.2. Time-resolved fluorescence measurements

Time-correlated single-photon counting measurements revealed the fluorescence lifetimes of the FCPb complexes under the three conditions. The fluorescence decay kinetics are presented in Figure 2. The results are summarized in Table 1. sFCPb, which is more homogeneous than the other two samples, exhibited a monoexponential fluorescence decay with an average lifetime of 3.9 ns. For qFCPb and plFCPb at least two exponential components were required to obtain a satisfactory fit, which can be explained by the size heterogeneity of the samples. For qFCPb, the predominant fluorescence decay occurred within 90

ps, showing a substantial shortening of the lifetime. The average lifetime of the plFCPb complexes was only 2.6 times shorter than that of sFCPb but >11 times longer than that of qFCPb. The relatively small amount of quenching in plFCPb (as compared to qFCPb) can be explained by the milder quenching environment produced by the liposomes as opposed to detergent removal. The protein density inside the liposome is an important factor affecting the fluorescence lifetime of the complexes. A large protein density increases the probability of protein–protein interactions [14, 40]. Since plFCPb constitutes a heterogeneous sample with varying protein densities, the fast and slow lifetime components possibly refer to average fluorescence lifetimes of FCPb complexes within more densely packed and less densely packed liposomes, respectively. The two lifetime components of qFCPb can be similarly explained as averages related to large and small aggregate sizes.

Table 1: Fitted decay times and relative amplitudes of the fluorescence decay curves of the FCPb nonamers (sFCPb), FCPb aggregates (qFCPb), and FCPb nonamers incorporated into liposomes (plFCPb). τ_1 and τ_2 are the fluorescence lifetime components, A_1 and A_2 the corresponding amplitudes, and τ_{ave} the weighted average of the lifetimes.

Sample	τ_1/ns	A_1	τ_2/ns	A_2	τ_{ave}/ns
sFCPb	3.88	1	-	-	3.88
plFCPb	0.82	0.50	2.21	0.50	1.51
qFCPb	0.09	0.97	1.28	0.03	0.13

3.3. Transient absorption spectroscopy

3.3.1 Global analysis

TA spectra were collected upon excitation at 680 nm. At this wavelength, Chl-a is excited selectively and the lowest-energy (i.e. red-most) Chls-a are excited with higher probability. To study the excited-state dynamics of Chl-a, we first analyzed the TA data globally using a sequential kinetic scheme. The resulting Evolution-Associated Difference Spectra (EADS) describe the dynamics of a mixture of spectroscopic species.

For the sFCPb data measured at 10 nJ/pulse pump energy, at least three components were needed to obtain a satisfactory fit. The corresponding EADS are presented in Figure 3(a). The initial component (1, black) appeared immediately after photoexcitation (i.e. at time zero) and evolved into the second EADS (2, red) in 5 ps. Its spectrum features an intense negative band peaking at 673 nm, which results from ground state bleach (GSB) and stimulated emission (SE) involving the Q_y transition of the red-most Chl-a pigments. The three positive signals peaking at 491nm, 600 nm and 642 nm are attributed to excited-state absorption (ESA) of Chl-a, because these signals are present immediately after photoexcitation and Chl-c and Fx are negligibly excited at 680 nm. In a transient-absorption study on LHCII where Chl-a was selectively excited at 675 nm, a broad ESA band with a peak position between 530 nm and 550 nm was resolved and similarly attributed to Chl-a [41]. The latter band is likely analogous to the broad Chl-a ESA band near 500 nm in Figure 3 and is red-shifted due to

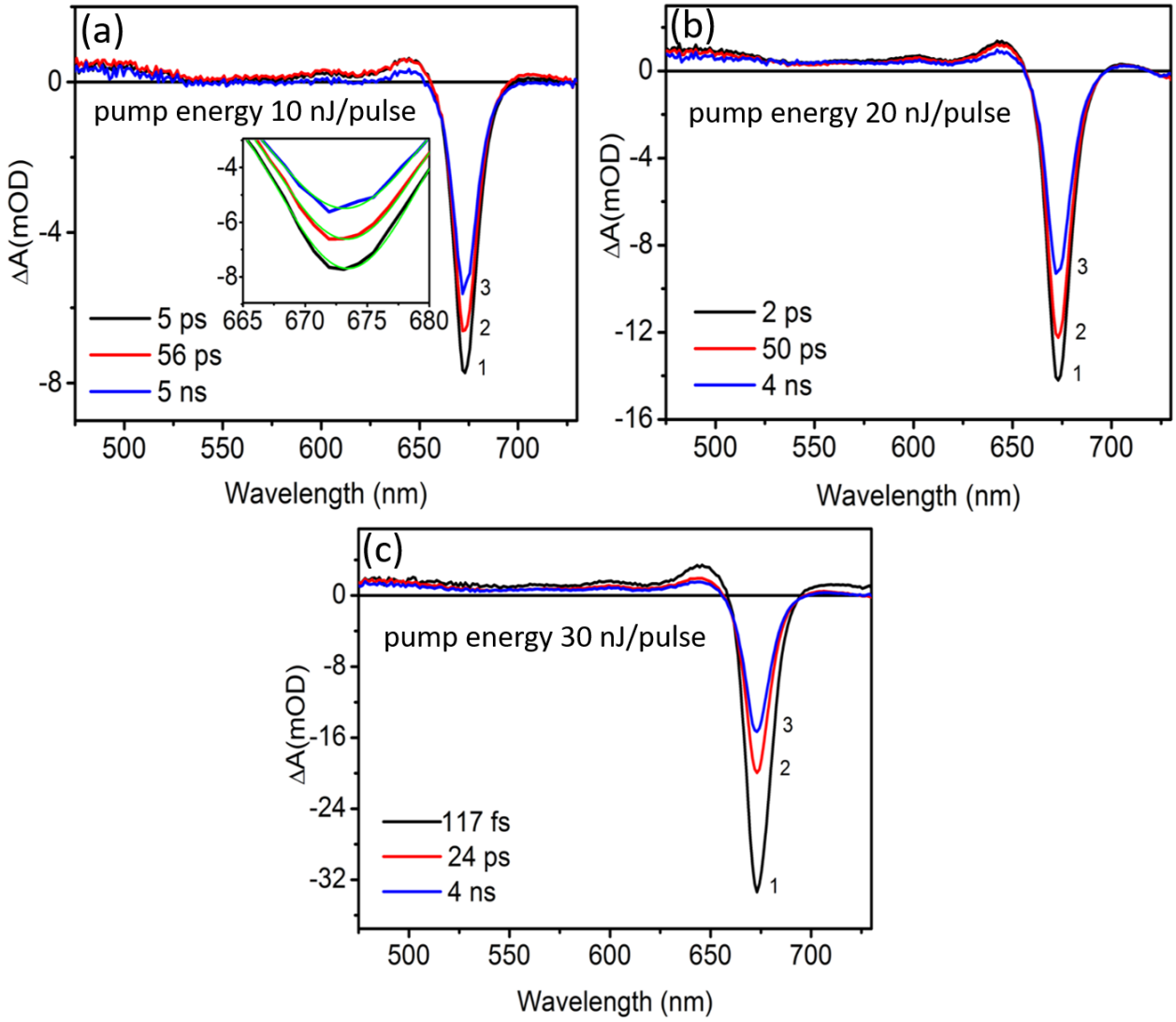

Figure 3: EADS and their lifetimes obtained by a sequential scheme in global analysis of the transient absorption data of the Chl-a excited state of sFCPb after pumping at (a) 10, (b) 20 and (c) 30 nJ/pulse. See text for details about the properties and possible origin of each of spectrum. Inset in (a) shows a magnification of the GSB/SE region and Gaussian fits (green) of the peaks within the displayed wavelength region.

the different coupling strengths amongst the Chls and between Chls-a and carotenoids in LHCII as opposed to FCPb. The 0.8 nm blue-shifted GSB/SE peak of the second EADS as compared to that of the first EADS Figure3 (a), inset) is explained by uphill energy redistribution amongst the Chls-a after being pumped at 680 nm, which is about 10 nm red-shifted compared to the absorption maximum of those Chls (Figure 1). This spectral shift, together with the decay time of the first EADS, indicates that the first EADS represents mainly excitation energy equilibration between Chl-a clusters with differing energies, i.e. different spectral pools. The second and third EADS exhibit similar features as the first EADS. The second spectrum takes 56 ps to decay into the third and final EADS (3, blue), which in turn relaxes into the ground state in 5 ns, a process attributed to spontaneous decay of Chl-a, mainly due to fluorescence emission and intersystem crossing. The amplitude of the GSB/SE

band decreases during evolution to both the second and third EADS. This can be explained by S-S annihilation (*vide infra*) and likely also a small degree of excitation quenching that manifests as fluorescence blinking in single molecule studies [29]. The additional 1 nm blue-shift from the second to the third EADS (Figure 3(a), inset) indicates that uphill energy equilibration is not completed after 5 ps. We attribute this to re-equilibration after S-S annihilation that involves mostly the blue spectral pool of Chls.

The results from higher pump intensities are displayed in Figures 3(b) and (c). Three EADS were again required to fit the data and the spectral features are similar to those displayed in Figure 3(a). In Figure 3(b), shortening of the decay lifetime of the first EADS as compared to Figure 3(a) can be explained by S-S annihilation, while the substantially shortened lifetime of the same EADS in Figure 3(c) suggests that an additional ultrafast process was resolved, likely vibrational cooling within Chl-a excited states [30]. The second EADS in Figure 3(b) has a similar decay time as that of Figure 3(a), suggesting that S-S annihilation plays a minor role on this timescale. For all three pump energies, the lifetime of the last EADS is comparable to τ_{ave} for sFCPb in Table 1, suggesting only a small degree of annihilation and quenching in the complexes.

Table 2: Fitted decay times of the maximum TA signal of sFCPb near 673 nm, using Equation (2). n_0 is the initial number of excitations per pulse, τ is the lifetime of an exponential decay process, and γ is the S-S annihilation rate.

Pump energy	n_0	γ^{-1} /ps	τ/ps
10 nJ/pulse	1.22 ± 0.04	25.0 ± 0.1	4.00
20 nJ/pulse	2.31 ± 0.07	25.0 ± 0.1	1.72
30 nJ/pulse	9.41 ± 0.22	25.0 ± 0.1	0.20

To verify the timescale and significance of S-S annihilation in the isolated FCPb complexes, we calculated its lifetime and amplitude using Equation (2). The kinetics of the sFCPb TA data at 10, 20 and 30 nJ/pulse were monitored at 673 nm and fitted simultaneously using Equation (2) (Figure 4), with the fitting results summarized in Table 2. For all three pump energies, an annihilation time constant of 25 ps was obtained and an additional, shorter lifetime component was resolved, the latter of which scaled inversely with the pump energy and compared well with the lifetimes of the first EADS in Figure 3 for corresponding data. It is important to note that fitting of the three traces separately produced very similar results. S-S annihilation is expected to be more enhanced in plFCPb and qFCPb complexes due to their increased number of connected pigments as compared to sFCPb.

The EADS for plFCPb at a pump energy of 10 nJ/pulse were also best fitted with three kinetic components (Figure 5(a)). The overall structure and band positions of the three EADS are similar to those for sFCPb but the altered decay times signify important differences in the underlying kinetics. Compared to sFCPb, the first EADS (1, black) decayed somewhat faster. This can in part be explained by an increased amount of S-S annihilation due to an enlarged absorption cross-section in liposomes

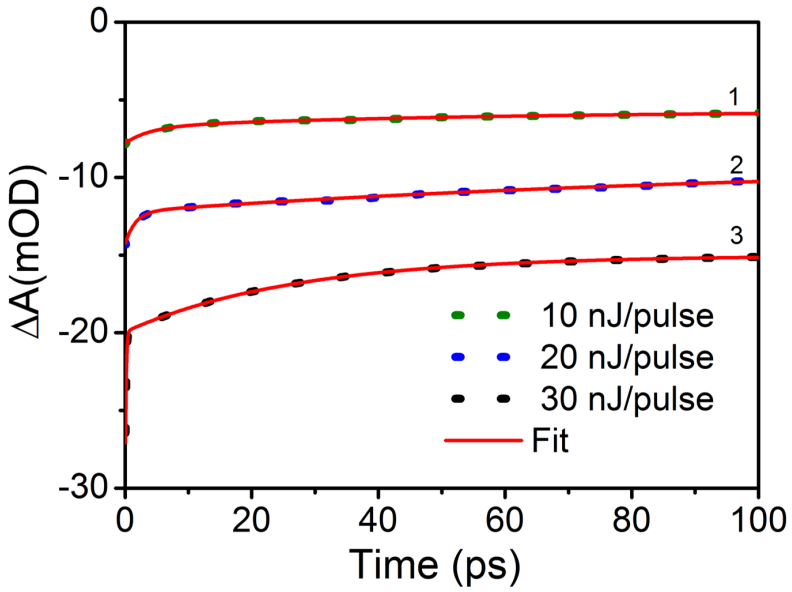

Figure 4: Transient kinetics monitored at maximum of the GSB/SE peak of sFCPb near 673 nm, for 10 nJ/pulse (green), 20 nJ/pulse (blue), and 30 nJ/pulse (black) excitations. The fit (red line) was obtained using Equation 2.

containing densely packed FCPb complexes, which constitute larger energetically connected domains than in the case of well-separated, solubilized complexes. The fluorescence lifetime results of plFCPb in Table 1 point to the presence of a slow and a fast quencher. Since annihilation was negligible in the lifetime study, there should be an additional quencher with decay dynamics strongly overlapping with that of annihilation and thus indiscriminable from the global analysis. The first EADS is again assigned to equilibration between the Chl-a spectral pools, as supported by the blue-shift of the second EADS (2, red). The small blue-shift of the third EADS (3, blue) suggests that the second EADS is again related to uphill re-equilibration following quenching of Chl-a with somewhat higher energies. Faster decay of the third EADS as compared to Figure 3(a) points to the presence of a slow quenching process. The considerably longer lifetime of the second EADS than in the case of sFCPb suggests a relatively long lifetime of the slow quenching process, in agreement with the fluorescence lifetime study (Table 1). Energy redistribution was also slowed down in the energetically coupled FCPb complexes inside the liposomes.

A new negative feature appeared in the third EADS of plFCPb from 680 nm to beyond 710 nm. Normalization of the spectra reveals that the second EADS also displays this feature with a small amplitude (Figure S2(a)). This low-energy feature does not manifest in the results of sFCPb for any of the pump energies and therefore suggests a new state induced by the lipid environment. Its prominence in the third and final EADS suggests that it is related to the slow quencher. This feature also explains the enhancement in the red tail of the Q_y band of the steady-state absorption spectrum (Figure1 (a) inset). The fitting residuals of the EADS shown in Figure S3 indicate that the red feature signifies a real signal.

For qFCPb pumped with the same energy, two kinetic components already provided a satisfactory fit of the EADS (Figure

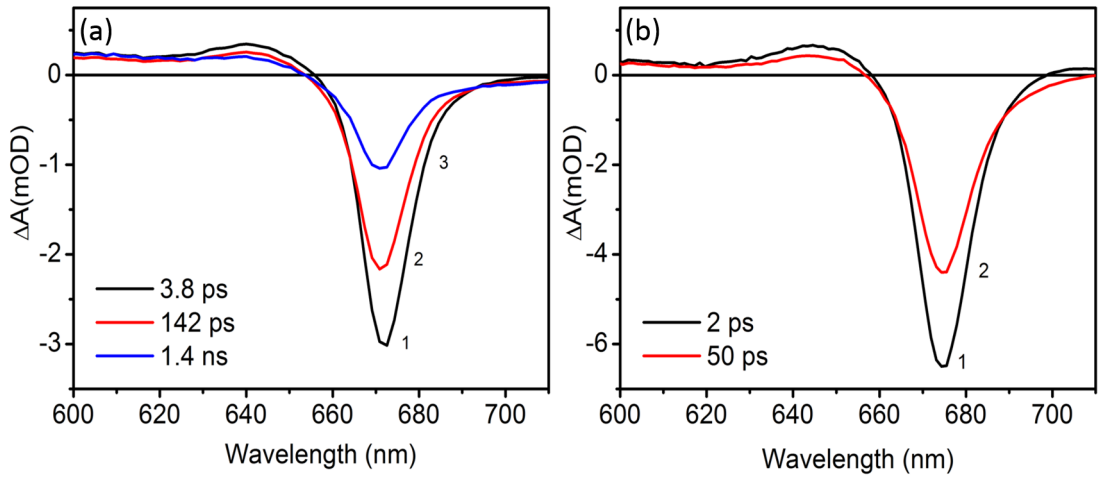

Figure 5: EADS and their lifetimes obtained by a sequential scheme in global analysis of the transient absorption data of (a) plFCPb and (b) qFCPb measured at 10 nJ/pulse pump energy. See text for details about the properties and possible origin of each spectrum.

5(b)). The main spectral features are similar to those for the other two samples. The faster decay of the first EADS (1, black) can be explained by annihilation and a fast quenching process like for plFCPb, considering again that the lifetime results of qFCPb suggest the presence of a slow and faster quenching process (Table 1), with the fast process strongly dominating. The average number of complexes forming an aggregate is expected to be significantly larger than the average number of strongly coupled complexes inside a liposome. It is also likely that the complexes are more strongly connected in an aggregate than inside a liposome. The short lifetime of the second and final EADS (2, red) indicates that the complexes are strongly quenched, in agreement with their short average fluorescence lifetime (Table 1). The second EADS displays a similar red feature between 680 and 710 nm as observed for plFCPb (see also the normalized spectrum in (Figure S2(a)), suggesting again formation of a new spectroscopic state related to the slow quencher. This red feature may similarly be connected with the slight broadening in the tail of the Q_y band in Figure 1. In a previous study, FCPa aggregates were observed to display a similar red feature on a timescale of several tens to hundreds of picoseconds [30].

3.3.2 Target analysis

Although a global analysis of the TA data of plFCPb and qFCPb failed to reveal the nature of the fast quenching process, our annihilation study clearly indicated the presence of annihilation, while the (free of S-S annihilation) fluorescence lifetime study suggested that an additional fast quenching channel should exist. We applied target analysis to the plFCPb and qFCPb data to determine if this is indeed the case. Target analysis furthermore reveals the quantitative contributions of the fast and slow quenching processes and provides the spectra and rates of the various energy transfer and dissipation processes. We started with the simplest kinetic scheme: Model A containing two compartments, shown in Figure 6(a). The compartments,

Chl1 and Chl2, describe the singlet excited states of red and blue absorbing Chl-a pools, with peak wavelengths at 673 and 671 nm, respectively. Their energy is quenched via two different quenching channels, q_1 and q_2, with rate constants k_1 and k_4, respectively, initially estimated from the last EADS in Figure 5. The distinct spectroscopic signatures of the two quenchers identified from global analysis suggest that the two quenchers are distinct and therefore independent. The initial populations of the two compartments were estimated from the global analysis results, which show that the ratio of the GSB/SE amplitude of Chl1 to that of Chl2 is ˜1.5, and the energy transfer from Chl1 to Chl2 is faster than the back transfer. k_2 and k_3 are the rate constants of energy equilibration between the two compartments, the initial values of which were estimated from the lifetime of the first EADS. It is not necessary to include in the model a description of long-lived components such as triplet and unquenched singlet states due to their absence in the global analysis results.

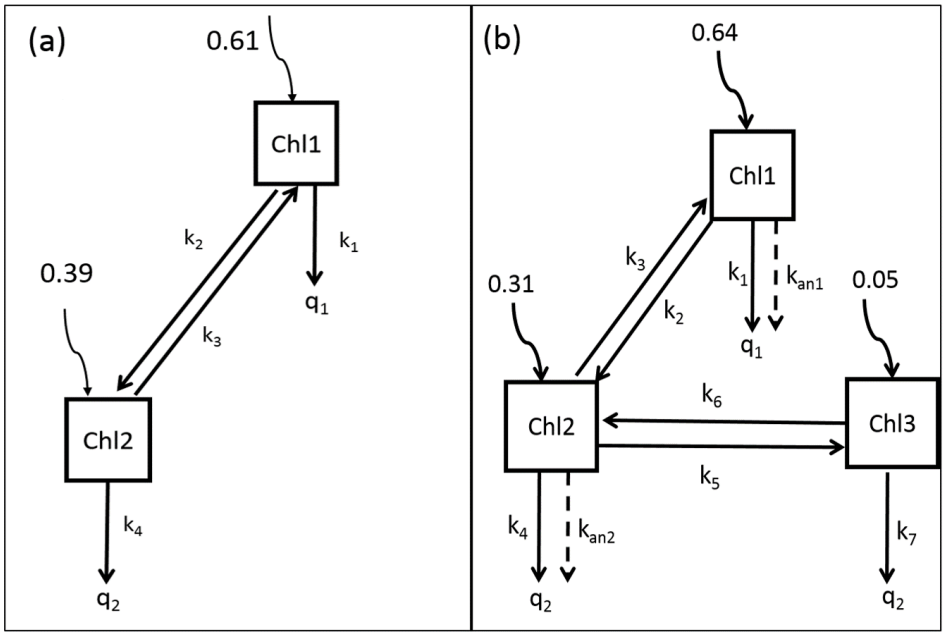

Figure 6: Compartment schemes used for target analysis to model the excited state dynamics of Chl-a in FCPb, using (a) two compartments (Model A) and (b) three compartments (Model B). Chl1, Chl2 and Chl3 are the compartments, k_{i} $(\mathrm{i} = 1, .., 7)$ the rate constants, k_{an1} and k_{an2} the annihilation rate constants, and q_1 and q_2 represent quenchers. The excitation probability of each compartment is shown.

The Species-Associated Difference Spectra (SADS) are the spectra of the molecular species associated with the two compartments, as obtained from target analysis. The SADS of plFCPb and qFCPb for Model A are shown in Figure 7(a) and (b), respectively, and the rate constants of the excited-state dynamics are summarized in Table 3. Table 4 shows the changes in population amplitudes of the two compartments at the lifetimes of the two SADS with respect to the initial populations. These values provide a useful measure of the overall direction of excitation energy transfer resulting from re-equilibration at different timescales due to quenching and annihilation processes. A negative sign denotes a decrease in the initial population

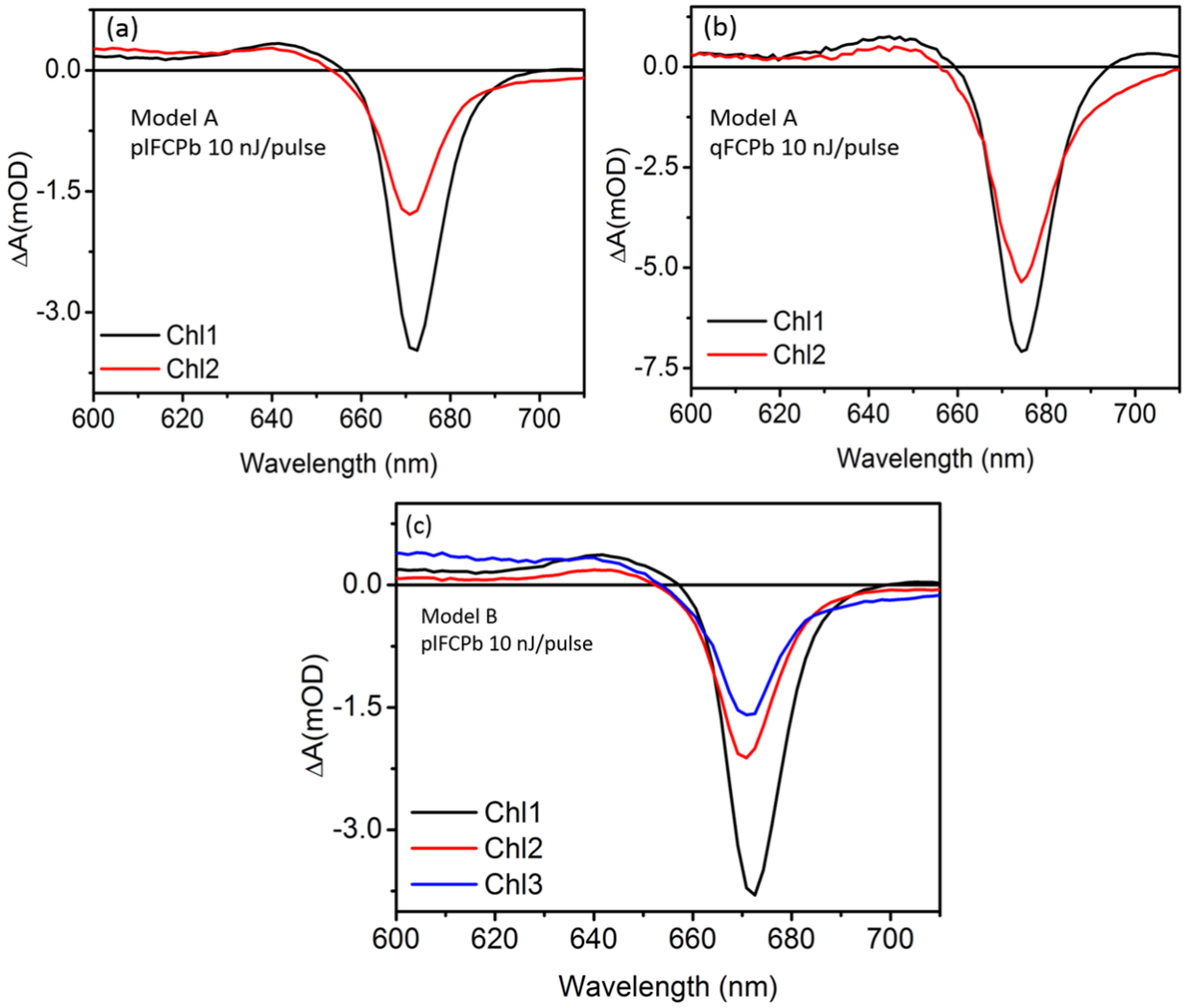

Figure 7: SADS of the Chl-a excited states using Model A for plFCPb (a) and qFCPb (b), and Model B for plFCPb (c).

of the compartment (i.e. recovery of a signal), while a positive value indicates growth of the population. For plFCPb, at 5 ps after photoexcitation the loss in the Chl1 population is only a fraction greater than the gain in the Chl2 population. This stems from the rate k_1 of the fast quenching channel q_1 being significantly slower than the equilibration rates k_2 and k_3, in combination with the result that the values of k_2 and k_3 are comparable (Table 3). The population shift to Chl2 explains the blue-shifted SADS of this compartment. After 650 ps, the population of both compartments has decreased, where that of Chl1 is significantly smaller due to equilibration to Chl2 as well as quenching channel q_1 being significantly faster than q_2. The SADS of Chl2 displays a long red tail beyond 680 nm (Figure 7(a)), indicating population of redder states.

For qFCPb, equilibration between Chl1 and Chl2 occurred faster than for plFCPb. This can be explained by the stronger connectivity between individual FCPb complexes forming an aggregate than between those inside a liposome. In addition,

aggregation may also induce changes inside individual FCPb complexes, such as small shifts in particular exciton energies and/or compression of the complexes. Both quenching processes occur considerably faster in the qFCPb model than for plFCPb, in agreement with the significant shortening of the associated EADS lifetimes in Figure 5(b). It is of note that k_1 is greater than k_2 and k_3, in contrast to the situation for plFCPb, highlighting the dominance of quenching process q_1. Moreover, the SADS of Chl2 also shows a red tail that is even stronger in qFCPb than in plFCPb.

The results from Model A suggest that the blue-absorbing Chl-a pool is associated with the strongly red-shifted state (absorbing beyond 680 nm) and confirm that the far-red feature is associated with a quenched state. The three lifetimes resolved from the EADS of plFCPb motivated the addition of a third compartment (Chl3) to our target model. This is done in Model B (Figure 6(b)). Simultaneous analysis of the data obtained at two different pump energies (6 nJ/pulse and 10 nJ/pulse) enabled us to decouple S-S annihilation from the two quenching processes. Annihilation was expected to affect the decay of Chl1 and Chl2. The initial values of the equilibration rates were obtained from Model A.

Since the far-red states feature on a relatively long timescale, Chl3 is expected to be strongly coupled with Chl2 and only weakly coupled with Chl1. Moreover, the energy in Chl3 is considered to be quenched through the same channel as for Chl2, involving q_2, albeit at a different rate due to the different nature of this state. This is because of the strong coupling between Chl2 and Chl3 compartments. Equilibration between Chl1 and Chl2 is established through rate constants k_2 and k_3, while equilibration between Chl2 and Chl3 is determined by k_5 and k_6. Due to the weak coupling between Chl1 and Chl3, equilibration between them is expected to be significantly slower than for the other processes and, for simplification, the associated rates were omitted from the model. The rates k_1, k_4, k_{an1} and k_{an2} were kept free, while all other rates were kept the same for the two data sets.

Table 3: Decay rate constants (in ns^{-1}) for plFCPb and qFCPb obtained from target analysis with Model A.

Sample	k_1	k_2	k_3	k_4
plFCPb	20	137	123	1
qFCPb	914	270	114	7

Table 4: Changes in population amplitudes of Chl1 and Chl2 compartments monitored at two times for plFCPb and qFCPb obtained with Model A. A negative sign indicates a decrease and a positive sign an increase.

Sample	plFCPb		qFCPb	
Lifetime (ps)	5	650	3	45
Chl1	-0.27	-0.79	-0.38	-0.52
Chl2	+0.23	-0.20	+0.14	-0.13

Upon photoexcitation, the Chl1 compartment is more populated than the other two compartments. Initially, the population

Table 5: Equilibration, decay and annihilation rate constants (in ns^{-1}) for plFCPb pumped with 6 nJ/pulse and 10 nJ/pulse energy, as obtained using Model B.

pump energy	k_1	k_2	k_3	k_4	k_5	k_6	k_7	k_{an1}	k_{an2}
6 nJ/pulse	6	226	127	8	33	1	1	10	13
10 nJ/pulse	7	227	127	9	33	1	1	55	18

of Chl1 is therefore expected to decrease due to equilibration, while those of Chl2 and Chl3 should increase, as observed in Table 6. The energy equilibration is affirmed by the blue-shift of the SADS of Chl2 and Chl3, as indicated in Figure 7(c). The rates of quenching of plFCPb pumped with 6 nJ/pulse and 10 nJ/pulse energies according to Model B are shown in Table 5. An initial population of 5% of Chl3 provided the best fit. This relatively small value in accordance with the slow formation of the far-red states, as suggested by the global analysis results. After 200 ps both Chl1 and Chl2 populations have decreased as compared to their amplitudes at 5 ps, while the Chl3 population has increased further. Decay of the Chl3 population, which is visible after 750 ps, was the slowest process of all and explains the relatively small red-shift of the Chl3 spectrum as compared to the Chl2 spectrum, because of equilibration to the far-state. From the starting values of the scaling parameter of the k-matrix we calculated that approximately 51% of the excitations were quenched via q_1, 16% via annihilation, and 33% via q_2 in the plFCPb sample, confirming that q_1 is the dominant quenching process. The results indicate that the kinetics of plFCPb are well-explained in terms of S-S annihilation in addition to two independent quenching processes, similarly to FCPa aggregates [30]. The same is expected for qFPCb. From the global and target analysis results, we conclude that the two fluorescence lifetime components of plFCPb (Table 1) are due to the presence of two different quenching channels.

Table 6: Changes in population amplitudes of Chl1, Chl2 and Chl3 compartments monitored at three times for plFCPb pumped at 10 nJ/pulse. These amplitudes are obtained from target analysis with Model B. Negative and positive signs again indicate a decrease and an increase in populations, respectively.

Lifetime (ps)	5	200	750
Chl1	-0.39	-0.59	-0.61
Chl2	+0.36	+0.10	-0.20
Chl3	+0.10	+0.18	-0.07

4. Discussion

Our analysis of the transient absorption data of plFCPb and qFCPb complexes points to the presence of two quenching channels in FCPb, both of which involve Chl-a. The first, fast channel (q_1) operates on a timescale of several tens of picoseconds for plFCPb and is expected to operate in qFCPb on a shorter timescale. The associated difference-absorption spectra do not exhibit a noticeable difference compared to the spectrum of solubilized FCPb. In this study, the majority of excitations de-

cayed via this channel. Since equilibration to the blue is visible in the GSB/SE band during and after energy loss via q_1, we can conclude that the Chls with the lowest energy (i.e. the terminal emitter Chls) are mostly involved and that the processes take place on multiple timescales. The second, slower quenching channel (q_2) occurs on a timescale of hundreds of picoseconds for plFCPb and down to tens of picoseconds for qFCPb. This quencher is responsible for enhanced population of states absorbing from 680 nm to beyond 710 nm and involves mainly the blue-shifted Chl-a pool.

The first quenching state has not been detected before for FCPb, likely because of the similarity of its spectral signature compared to that of the unquenched state. The characteristics of the second quencher are similar to those of a spectral state identified from a transient absorption study on FCPa aggregates [30]. Although a similar signal was absent from the Stark data of FCPb aggregates it was predicted to exist [27]. The signal of this quenched state has now been resolved in the present study and further kinetic information has been provided.

The involvement of a charge-transfer state is the best explanation for the large red-shift of the low-energy band identified from the Stark study and its strong response to an externally applied electrical field [27]. For photosystem I of plants, which exhibit similar low-energy states, it has been established that low-energy spectral states originate from a Chl dimer due to mixing between a charge-transfer state and one or more of the lowest exciton states [42, 43]. The low-energy emission states from plant LHCII aggregates as well as FCP aggregates have been proposed to originate from a similar mechanism, but involving Chls-a from adjacent complexes [25, 44]. However, states with similar properties have been observed from single, isolated LHCs from plant photosystem II [45, 46] and were related to the low-energy states of photosystem I LHCs [46], suggesting that the red states in isolated and aggregated LHCs of plants involve a Chl dimer within a complex instead of between different complexes.

Blue-absorbing Fx molecules are proposed to be located close to Chl-a molecules in the FCPs complexes similar to lutein molecules in LHCII [5, 47]. Association of the slow quencher with the blue Chl-a pool therefore suggests the involvement of one or more Fx molecules. Fx is characterized by a strong intramolecular charge-transfer (ICT) state coupled to the molecule's S_1 state to form a mixed S_1/ICT state [48,49]. In FCP, the latter state couples strongly to the Q_y exciton states of neighbouring Chls-a to give rise to ultrafast energy transfer [7, 20]. Due to this strong coupling and the 'availability' of a charge-transfer state, it is natural to assume that Fx's ICT state will mix into some of the Chl-a exciton states, thus giving rise to quenching and low-energy emission. This was also the explanation for the ˜694-nm emission state of FCPb in the Stark study [27].

In a TA spectroscopy study on solubilized and aggregated FCPa [30] very similar results were obtained as in the present study. Specifically, for aggregated FCPa, two quenchers in the Chl-a pool were identified in addition to annihilation, with almost

identical spectral signatures and transient dynamics as for FCPb. This leads us to conclude that the origin of the slow quencher (q_2) is the same in FCPa and FCPb and that FCPb has the same capability as FCPa to serve as a dissipater of excess excitation energy.

The NPQ-related spectral properties are therefore not unique to FCPa. This can be explained by the strong similarity of FCPa and FCPb in terms of protein sequence – and hence structural homology – as well as pigment composition [14]. *In vivo*, the two quenching channels are likely activated in FCPa upon aggregation in the membrane under NPQ conditions [14, 24, 25]. Although *in vitro* aggregation of FCPb is just as easily induced as for FCPa, it is very unlikely that FCPb aggregates are formed *in vivo*. A time-resolved fluorescence study on whole *Cyclotella meneghiniana* cells indicated that the FCPb signal shows no sign of quenching under NPQ conditions [24], and neither Dt content nor low pH values influence the fluorescence yield of FCPb, in stark contrast to FCPa [14]. Yet, FCPb seems to be an even more efficient energy dissipater than FCPa: in a similar TA study on FCPa [30], 15-times quenched FCPa aggregates were used, as opposed to 10-times quenched FCPb aggregates in the present study, but the quenching rates of those FCPa aggregates were significantly slower than for the FCPb aggregates reported here.

This prompts us to ask why FCPb is not involved with NPQ *in vivo*. To act as a useful regulator of excitation pressure, quenching of FCPs has to be highly regulated in order to avoid permanent NPQ. Use of a weaker quencher might be easier to control and thus fine-tune NPQ more easily.

Aggregation of FCPa is likely triggered by the glutamate residue on the lumenal side of the Lhcx and/or specific Lhcf polypeptides [14], which are probably sensitive to pH changes in the lumen and possibly also to binding of Dt in its vicinity. Fcp5, the sole component of FCPb, does not contain this specific glutamate [14]. The difference of such a single amino acid is probably sufficient to regulate the involvement of FCPa in qE and not FCPb, despite the fact that FCPb could equally well serve as an efficient dissipater of excess energy if a mechanism for *in vivo* FCPb aggregation existed. It has to be noted that FCPb complexes exist only in centric diatoms, whereas they are missing in pennate diatoms (like *Phaeodactylum tricornutum*) that also display a high NPQ capability. Use of FCPa is therefore sufficient for the fine regulation involved with qE.

The lipid environment produced very similar spectroscopic signatures as aggregation, suggesting that common quenching mechanisms are involved. In fact, there is sufficient motivation for considering the lipid environment a more suitable model for studies of (photoprotective) energy dissipation. First, in this study, lipid interaction induced only a relatively small degree of quenching while the quenching-related spectral signatures were pronounced. Specifically, the amount of quenching in plFCPb was significantly less than in qFCPb while the far-red signal related to the slow quencher in plFCPb was somewhat

more intense than for qFCPb. This observation indicates that the amplitude of the far-red spectral band is not related to the strength of quenching. Second, aggregates may introduce spectral artifacts: (i) *in vitro* aggregation using a detergent concentration below the critical micelle concentration, as frequently done [13,14], leads to uncontrolled aggregation, typically producing large, three-dimensional structures, unlike what is expected *in vivo*, (ii) the presence of even a small fraction of non-functional or denatured complexes may introduce additional energy traps and amplify the extent of quenching when bound to large aggregates, and (iii) aggregation produced with bio-beads can lead to the loss of pigments located peripherally in the complexes due to strong hydrophobic interactions, as observed in Figure 1 for qFCPb.

5. Conclusions

In this study, we were able to resolve two quenching channels in FCPb that are created when the complexes are aggregated and when they are incorporated in liposomes. The two quenching channels are associated with different molecular mechanisms and operate at different timescales. The first, fast quenching mechanism occurs on a timescale of tens of picoseconds within the red Chl-a pool. The second, slow quenching mechanism is characterized by a far-red absorption state and likely originates from an Fx S_1/ICT state mixed with a higher energy (blue) Chl-a exciton state. In addition, we calculated a singlet-singlet annihilation rate of 25 ps^{-1} in isolated FCPb complexes subjected to high excitation pulse energies. Our results show that FCPb aggregates are stronger quenchers than FCPa aggregates and FCPb therefore has the potential to quench excess excitations more efficiently than FCPa, yet FCPb does not play a role in qE because of its lack of Lhcx subunits and missing regulatory, pH-sensing amino acid residues. Motivations were given for why the proteoliposomes provide a better model system for energy-dissipation studies than aggregation. Finally, we conclude from this study that the presence of both excitation quenching and a far-red spectral signal *in vitro* is not sufficient evidence for any light-harvesting complex's participation in qE *in vivo*, because aggregated of FCPb exhibit these signatures but are not involved with qE.

6. Acknowledgments

The authors gratefully acknowledge Roberta Croce for the use of her TCSPC setup and biochemical laboratory. This work was supported by the National Research Foundation (NRF) of South Africa through grants no. 88653 and 106298 (H.M.A.M.E.) and grant no. N00500 (T.P.J.K.), the South Africa – VU University – Strategic Alliances (SAVUSA) Skill Programme (H.M.A.M.E.), the South African Institute of Physics Biophysics Initiative (H.M.A.M.E.); the Energy Institutional Research Theme and Research Development Programme of the University of Pretoria (T.P.J.K.), the Feodor-Lynen Fellowship of the Alexander von Humboldt Foundation (L.D.), Kerstin Pieper for experimental help in FCPb preparation (L.D), the Deutsche

Forschungsgemeinschaft (DFG) (Grant Bu 812/10-1) (C.B.), an Advanced Investigator Grant (267333, PHOTPROT) from the European Research Council (ERC) (R.v.G. and C.R.), and a grant from the Royal Netherlands Academy of Arts and Sciences (KNAW) (R.v.G.).

References

[1] C. Wilhelm, C. Büchel, J. Fisahn, R. Goss, T. Jakob, J. LaRoche, J. Lavaud, M. Lohr, U. Riebesell, K. Stehfest, K. Valentin, and P. G. Kroth, "The regulation of carbon and nutrient assimilation in diatoms is significantly different from green algae," *Protist*, vol. 157, no. 2, pp. 91 – 124, 2006.

[2] B. R. Green, E. Pichersky, and K. Kloppstech, "Chlorophyll a/b-binding proteins: an extended family," *Trends in biochemical sciences*, vol. 16, pp. 181–186, 1991.

[3] C. Büchel, "Fucoxanthin-chlorophyll proteins in diatoms: 18 and 19 kDa subunits assemble into different oligomeric states," *Biochemistry*, vol. 42, no. 44, pp. 13027–13034, 2003.

[4] A. Beer, K. Gundermann, J. Beckmann, and C. Büchel, "Subunit composition and pigmentation of fucoxanthin-chlorophyll proteins in diatoms: evidence for a subunit involved in diadinoxanthin and diatoxanthin binding," *Biochemistry*, vol. 45, no. 43, pp. 13046–13053, 2006.

[5] L. Premvardhan, B. Robert, A. Beer, and C. Büchel, "Pigment organization in fucoxanthin chlorophyll a/c 2 proteins (FCP) based on resonance raman spectroscopy and sequence analysis," *Biochimica et Biophysica Acta (BBA)-Bioenergetics*, vol. 1797, no. 9, pp. 1647–1656, 2010.

[6] Z. Liu, H. Yan, K. Wang, T. Kuang, J. Zhang, L. Gui, X. An, and W. Chang, "Crystal structure of spinach major light-harvesting complex at 2.72 $\AA$ resolution," pp. 287–92, 2004.

[7] E. Papagiannakis, I. H. van Stokkum, H. Fey, C. Büchel, and R. van Grondelle, "Spectroscopic characterization of the excitation energy transfer in the fucoxanthin-chlorophyll protein of diatoms," *Photosynthesis Research*, vol. 86, no. 1, pp. 241–250, 2005.

[8] A. Röding, E. Boekema, and C. Büchel, "The structure of FCPb, a light-harvesting complex in the diatom cyclotella meneghiniana," *Photosynthesis Research*, pp. 1–9, 2016.

[9] B. Bailleul, A. Rogato, A. De Martino, S. Coesel, P. Cardol, C. Bowler, A. Falciatore, and G. Finazzi, "An atypical member of the light-harvesting complex stress-related protein family modulates diatom responses to light," *Proceedings of the National Academy of Sciences*, vol. 107, no. 42, pp. 18214–18219, 2010.

[10] J. Lavaud, B. Rousseau, H. J. Van Gorkom, and A.-L. Etienne, "Influence of the diadinoxanthin pool size on photoprotection in the marine planktonic diatom phaeodactylum tricornutum," *Plant Physiology*, vol. 129, no. 3, pp. 1398–1406, 2002.

[11] B. Demmig-Adams and W. W. Adams III, "The role of xanthophyll cycle carotenoids in the protection of photosynthesis," *Trends in Plant science*, vol. 1, no. 1, pp. 21–26, 1996.

[12] M. Olaizola, J. La Roche, Z. Kolber, and P. G. Falkowski, "Non-photochemical fluorescence quenching and the diadinoxanthin cycle in a marine diatom," *Photosynthesis Research*, vol. 41, no. 2, pp. 357–370, 1994.

[13] K. Gundermann and C. Büchel, "The fluorescence yield of the trimeric fucoxanthin-chlorophyll-protein FCPa in the diatom cyclotella meneghiniana is dependent on the amount of bound diatoxanthin," *Photosynthesis Research*, vol. 95, no. 2-3, pp. 229–235, 2008.

[14] K. Gundermann and C. Büchel, "Factors determining the fluorescence yield of fucoxanthin-chlorophyll complexes (FCP) involved in non-photochemical quenching in diatoms," *Biochimica et Biophysica Acta (BBA)-Bioenergetics*, vol. 1817, no. 7, pp. 1044–1052, 2012.

[15] P. Horton, A. Ruban, D. Rees, A. Pascal, G. Noctor, and A. Young, "Control of the light-harvesting function of chloroplast membranes by aggregation of the LHCII chlorophyll-protein complex," *FEBS letters*, vol. 292, no. 1, pp. 1–4, 1991.

[16] P. Horton, M. Wentworth, and A. Ruban, "Control of the light harvesting function of chloroplast membranes: The LHCII-aggregation model for non-photochemical quenching," *Febs Letters*, vol. 579, no. 20, pp. 4201–4206, 2005.

[17] P. Horton, A. V. Ruban, and R. G. Walters, "Regulation of light harvesting in green plants (indication by nonphotochemical quenching of chlorophyll fluorescence).," *Plant Physiology*, vol. 106, no. 2, p. 415, 1994.

[18] P. Müller, X.-P. Li, and K. K. Niyogi, "Non-photochemical quenching. A response to excess light energy," *Plant Physiology*, vol. 125, no. 4, pp. 1558–1566, 2001.

[19] A. V. Ruban, R. Berera, C. Ilioaia, I. H. Van Stokkum, J. T. Kennis, A. A. Pascal, H. Van Amerongen, B. Robert, P. Horton, and R. Van Grondelle, "Identification of a mechanism of photoprotective energy dissipation in higher plants," *Nature*, vol. 450, no. 7169, pp. 575–578, 2007.

[20] N. Gildenhoff, S. Amarie, K. Gundermann, A. Beer, C. Büchel, and J. Wachtveitl, "Oligomerization and pigmentation dependent excitation energy transfer in fucoxanthin-chlorophyll proteins," *Biochimica et Biophysica Acta (BBA)-Bioenergetics*, vol. 1797, no. 5, pp. 543–549, 2010.

[21] G. Öquist and N. P. Huner, "Photosynthesis of overwintering evergreen plants," *Annual Review of Plant Biology*, vol. 54, no. 1, pp. 329–355, 2003.

[22] Y. Tang, X. Wen, Q. Lu, Z. Yang, Z. Cheng, and C. Lu, "Heat stress induces an aggregation of the light-harvesting complex of photosystem II in spinach plants," *Plant physiology*, vol. 143, no. 2, pp. 629–638, 2007.

[23] A. V. Ruban, *The photosynthetic membrane: molecular mechanisms and biophysics of light harvesting*. John Wiley & Sons, 2012.

[24] V. U. Chukhutsina, C. Büchel, and H. van Amerongen, "Disentangling two non-photochemical quenching processes in cyclotella meneghiniana by spectrally-resolved picosecond fluorescence at 77K," *Biochimica et Biophysica Acta (BBA)-Bioenergetics*, vol. 1837, no. 6, pp. 899–907, 2014.

[25] Y. Miloslavina, I. Grouneva, P. H. Lambrev, B. Lepetit, R. Goss, C. Wilhelm, and A. R. Holzwarth, "Ultrafast fluorescence study on the location and mechanism of non-photochemical quenching in diatoms," *Biochimica et Biophysica Acta (BBA)-Bioenergetics*, vol. 1787, no. 10, pp. 1189–1197, 2009.

[26] I. Grouneva, T. Jakob, C. Wilhelm, and R. Goss, "Influence of ascorbate and ph on the activity of the diatom xanthophyll cycle-enzyme diadinoxanthin de-epoxidase," *Physiologia Plantarum*, vol. 126, no. 2, pp. 205–211, 2006.

[27] M. Wahadoszamen, A. Ghazaryan, H. E. Cingil, A. M. Ara, C. Büchel, R. van Grondelle, and R. Berera, "Stark fluorescence spectroscopy reveals two emitting sites in the dissipative state of FCP antennas," *Biochimica et Biophysica Acta (BBA)-Bioenergetics*, vol. 1837, no. 1, pp. 193–200, 2014.

[28] B. Lepetit, R. Goss, T. Jakob, and C. Wilhelm, "Molecular dynamics of the diatom thylakoid membrane under different light conditions," *Photosynthesis research*, vol. 111, no. 1-2, pp. 245–257, 2012.

[29] T. P. Krüger, P. Malỳ, M. T. Alexandre, T. Mančal, C. Büchel, and R. van Grondelle, "How reduced excitonic coupling enhances light harvesting in the main photosynthetic antennae of diatoms," *Proceedings of the National Academy of Sciences*, p. 201714656, 2017.

[30] C. Ramanan, R. Berera, K. Gundermann, I. van Stokkum, C. Büchel, and R. van Grondelle, "Exploring the mechanism (s) of energy dissipation in the light harvesting complex of the photosynthetic algae cyclotella meneghiniana," *Biochimica et Biophysica Acta (BBA)-Bioenergetics*, vol. 1837, no. 9, pp. 1507 – 1513, 2014.

[31] A. Natali, J. M. Gruber, L. Dietzel, M. C. Stuart, R. van Grondelle, and R. Croce, "Light-harvesting complexes (LHCs) cluster spontaneously in membrane environment leading to shortening of their excited state lifetimes," *Journal of Biological Chemistry*, vol. 291, no. 32, pp. 16730–16739, 2016.

[32] L. Provasoli, J. McLaughlin, and M. Droop, "The development of artificial media for marine algae," *Archiv für Mikrobiologie*, vol. 25, no. 4, pp. 392–428, 1957.

[33] B. Van Oort, A. Amunts, J. W. Borst, A. Van Hoek, N. Nelson, H. Van Amerongen, and R. Croce, "Picosecond fluorescence of intact and dissolved PSI-LHCI crystals," *Biophysical journal*, vol. 95, no. 12, pp. 5851–5861, 2008.

[34] R. Berera, R. van Grondelle, and J. T. Kennis, "Ultrafast transient absorption spectroscopy: principles and application to photosynthetic systems," *Photosynthesis research*, vol. 101, no. 2-3, pp. 105–118, 2009.

[35] C. C. Gradinaru, I. H. M. van Stokkum, A. A. Pascal, R. van Grondelle, and H. van Amerongen, "Identifying the pathways of energy transfer between carotenoids and chlorophylls in LHCII and CP29. a multicolor femtosecond pump-probe study," *The Journal of Physical Chemistry B*, vol. 104, no. 39, pp. 9330–9342, 2000.

[36] D. Rutkauskas, J. Chmeliov, M. Johnson, A. Ruban, and L. Valkunas, "Exciton annihilation as a probe of the light-harvesting antenna transition into the photoprotective mode," *Chemical Physics*, vol. 404, pp. 123–128, 2012.

[37] J. Larsen, B. Brüggemann, T. Polivka, V. Sundström, E. Akesson, J. Sly, and M. J. Crossley, "Energy transfer within zn–porphyrin dendrimers, study of the singlet-singlet annihilation kinetics," *The Journal of Physical Chemistry A*, vol. 109, no. 47, pp. 10654–10662, 2005.

[38] J. Snellenburg, S. Laptenok, R. Seger, K. Mullen, and I. V. Stokkum, "Glotaran: a java-based graphical user interface for the R package TIMP," *Journal of Statistical Software*, vol. 49, no. 3, 2012.

[39] I. H. van Stokkum, D. S. Larsen, and R. van Grondelle, "Global and target analysis of time-resolved spectra," *Biochimica et Biophysica Acta (BBA) - Bioenergetics*, vol. 1657, no. 23, pp. 82 – 104, 2004.

[40] I. Moya, M. Silvestri, O. Vallon, G. Cinque, and R. Bassi, "Time-resolved fluorescence analysis of the photosystem II antenna proteins in detergent micelles and liposomes," *Biochemistry*, vol. 40, no. 42, pp. 12552–12561, 2001. PMID: 11601979.

[41] C. C. Gradinaru, R. Van Grondelle, and H. Van Amerongen, "Selective interaction between xanthophylls and chlorophylls in LHCII probed by femtosecond transient absorption spectroscopy," *The Journal of Physical Chemistry B*, vol. 107, no. 16, pp. 3938–3943, 2003.

[42] R. Croce, A. Chojnicka, T. Morosinotto, J. A. Ihalainen, F. Van Mourik, J. P. Dekker, R. Bassi, and R. Van Grondelle, "The low-energy forms of photosystem I light-harvesting complexes: spectroscopic properties and pigment-pigment interaction characteristics," *Biophysical journal*, vol. 93, no. 7, pp. 2418–2428, 2007.

[43] E. Romero, M. Mozzo, I. H. Van Stokkum, J. P. Dekker, R. Van Grondelle, and R. Croce, "The origin of the low-energy form of photosystem I light-harvesting complex Lhca4: mixing of the lowest exciton with a charge-transfer state," *Biophysical journal*, vol. 96, no. 5, pp. L35–L37, 2009.

[44] Y. Miloslavina, A. Wehner, P. H. Lambrev, E. Wientjes, M. Reus, G. Garab, R. Croce, and A. R. Holzwarth, "Far-red fluorescence: A direct spectroscopic marker for LHCII oligomer formation in non-photochemical quenching," *FEBS letters*, vol. 582, no. 25-26, pp. 3625–3631, 2008.

[45] T. P. Krüger, V. I. Novoderezhkin, C. Ilioaia, and R. Van Grondelle, "Fluorescence spectral dynamics of single LHCII trimers," *Biophysical journal*, vol. 98, no. 12, pp. 3093–3101, 2010.

[46] T. P. Krüger, E. Wientjes, R. Croce, and R. van Grondelle, "Conformational switching explains the intrinsic multifunctionality of plant light-harvesting complexes," *Proceedings of the National Academy of Sciences*, vol. 108, no. 33, pp. 13516–13521, 2011.

[47] M. Di Valentin, C. Büchel, G. M. Giacometti, and D. Carbonera, "Chlorophyll triplet quenching by fucoxanthin in the fucoxanthin-chlorophyll protein from the diatom cyclotella meneghiniana," *Biochemical and biophysical research communications*, vol. 427, no. 3, pp. 637–641, 2012.

[48] D. Zigmantas, R. G. Hiller, F. P. Sharples, H. A. Frank, V. Sundstrom, and T. Polivka, "Effect of a conjugated carbonyl group on the photophysical properties of carotenoids," *Phys. Chem. Chem. Phys.*, vol. 6, pp. 3009–3016, 2004.

[49] L. Premvardhan, L. Bordes, A. Beer, C. Buchel, and B. Robert, "Carotenoid structures and environments in trimeric and oligomeric fucoxanthin chlorophyll a/c2 proteins from resonance raman spectroscopy," *The Journal of Physical Chemistry B*, vol. 113, no. 37, pp. 12565–12574, 2009.

[50] H. Schägger and G. Von Jagow, "Tricine-sodium dodecyl sulfate-polyacrylamide gel electrophoresis for the separation of proteins in the range from 1 to 100 kda," *Analytical biochemistry*, vol. 166, no. 2, pp. 368–379, 1987.

[51] M. Chevallet, S. Luche, and T. Rabilloud, "Silver staining of proteins in polyacrylamide gels," *Nature protocols*, vol. 1, no. 4, p. 1852, 2006.

7. Appendix A. Supplementary information

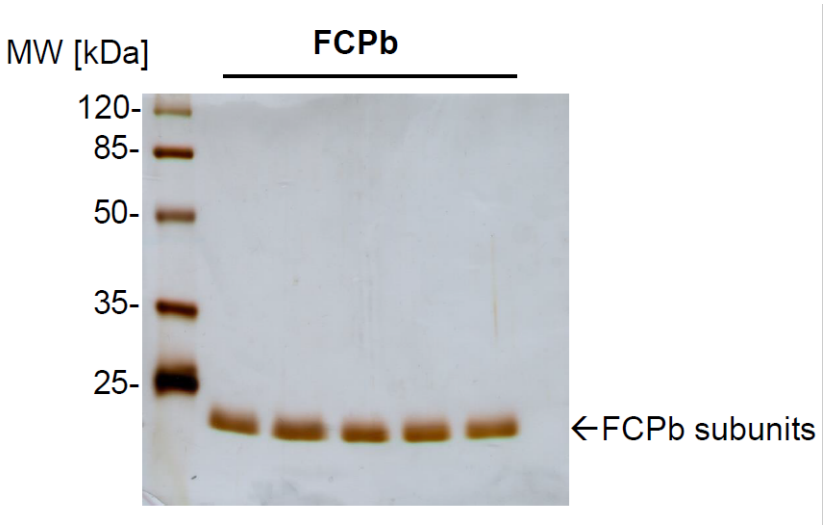

Figure S1: Separation of purified FCPb subunits. FCPb subunits were purified as described in the main manuscript. The image represents all batches of FCPb preparations used for the manuscript. The FCPb subunits migrate in a single band of 19 kDa [4]. FCPb corresponding to 0.5 μg Chl-a was loaded in each well. The gel electrophoresis was performed using a tris-tricine buffer system with 12% polyacrylamide according to Schägger and Jagow [50]. Silver staining procedure was based on Chevallet [51]

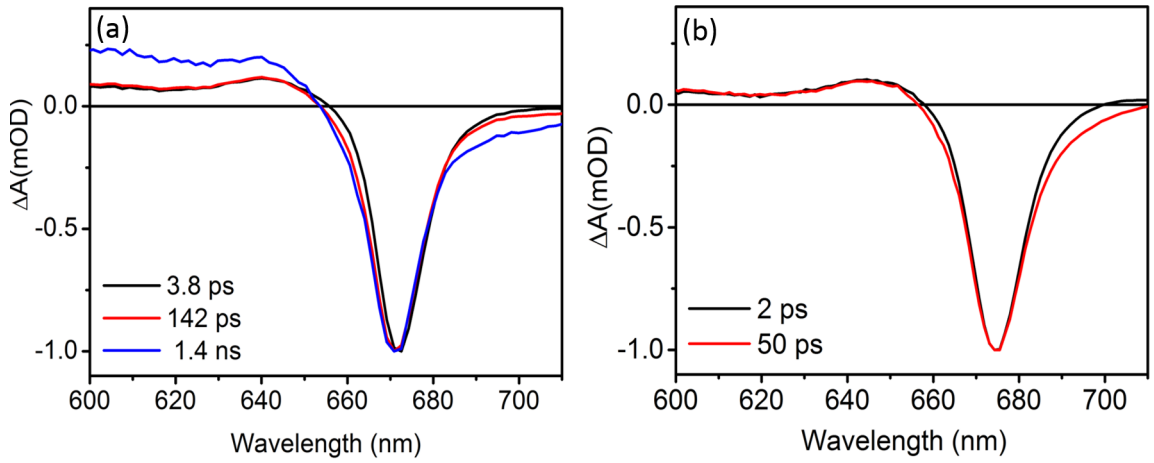

Figure S2: Normalized EADS spectra from the global analysis of plFCPb (a) and qFCPb (b) TA data, that correspond to EADS spectra in Figure 5. The normalized spectra clearly demonstrate the broadening from 680-710 nm on the last EADS spectra in Figures 5 (a) and (b).

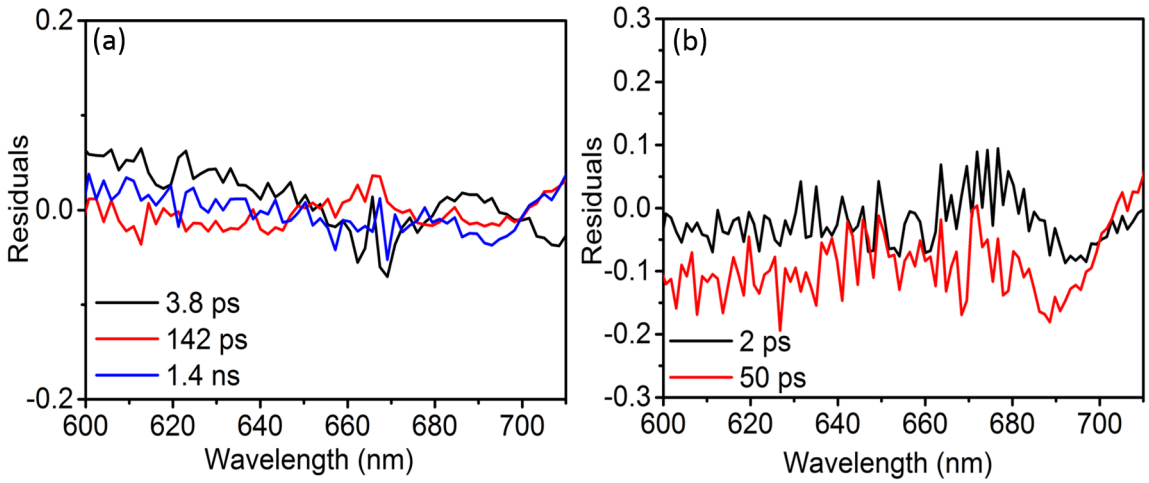

Figure S3: Residuals curves of the global analysis fit of the plFCPb (a) and qFCPb (b) TA data, that correspond to the plFCPb and qFCPb EADS spectra in Figure 5 (a) and (b), respectively. These residuals show no any particular pattern, which confirm that the broadening from 680-710 nm on the last EADS spectra in Figures 5 (a) and (b) are real signals.